Erschienen in: 4th International Symposium on Slow Dynamics in Complex Systems : Keep Going Tohoku / Michio Tokuyama ... (Hrsg.). - Melville, NY : AIP, American Inst. of Physics, 2013. - (AIP Conference Proceedings ; 1518). - S. 134-142. - ISBN 978-1-62993-682-6

Nonlinear rheological response of colloidal glass

M. Fuchs

Fachbereich Physik, Universität Konstanz, 78457 Konstanz, Germany

Abstract.
I review a first principles approach to the non-linear rheology of dense colloidal dispersions. Assuming homogeneous flow and neglecting hydrodynamic interactions, a theoretical description of the stresses, micro-structure, and particle motion close to a colloidal glass transition are developed. Results for large amplitude oscillatory shearing, step-strains, and other time-dependent transient deformation protocols provide a unifying description of the dispersion properties under general strains including non-stationary situations. Shear-thinning, plastic deformation and an-elastic behaviour are observed. Adding Brownian dynamics simulations, the shear-induced particle motion provides information on the microscopic transport mechanisms in the dense dispersions

Keywords: Rheology, colloidal dispersions, glass transition
PACS: 82.70.Dd, 64.70.Pf, 83.60.Df, 83.10.Gr

INTRODUCTION

The nonlinear response of complex materials provides a wealth of information on the internal mechanisms determining structural and transport properties. Soft materials are very susceptible to applied deformations and loads, which gives the name to this class of materials. Thus, it is fortunate that colloidal dispersions, a well investigated subclass of soft matter, exhibit glass transitions, which can be investigated in detail by optical and other microscopy techniques.

The colloidal glass states can easily be melted, deformed, and otherwise manipulated by external flow fields or loads. This provides unique access to the internal particle arrangements during vitrification, as the external forces can be chosen to interact with specific intrinsic transport processes. Micro-rheology can be mentioned as one example, where the force on a colloidal probe locally melts the glassy environment around the driven particle, and consequently the force caging a particle can be measured [1]. Additionally, the anomalous and heterogeneous motion when the particle is un-pinned at larger forces reveals itself [2].

Macro-rheology provides another, albeit more traditional, way to investigate the strength of the local elasticity under applied external flows. The history dependence of the rheological response already arises in the linear regime, where Boltzmann's principle leads to a Green-Kubo relation for the dispersion viscosity. More general, it leads to the frequency dependent linear moduli. The history dependence of the material can especially well be studied in time-dependent flows. Linear superposition principles are then known to fail, even though they still often form the basis for macroscopic constitutive modeling. Only recently, progress on a microscopic theory of the colloidal rheology at the glass transition has been made.

This conference proceedings' contribution reviews recent progress within a microscopic statistical mechanics framework, to capture the memory effects at the glass transition quantitatively. Results from theory are compared to Brownian dynamics simulations and experiments in model microgel dispersions, in order to establish the qualitative scenario, how glasses yield and plastically deform in flow.

MODE-COUPLING THEORY

Recently, the MCT of the glass transition [3] was generalized in an integration through transients approach [4, 5] to colloidal dispersions under homogeneous flow with arbitrary time-dependence [6, 7, 8, 9]. This yields a theory capturing shear-thinning, yielding, and plastic deformation and flow. We first review the approach following Ref. [10], and then we present results and comparisons characterizing the effects described.

ITT-MCT describes structural correlations using a transient density correlator $\Phi_{\mathbf{q}}(t,t')$ which encodes the relaxation of density fluctuations. They are taken to have equilibrium strength, and their dynamics is determined by the retarded stress correlations stored in the system and the strain accumulated, both in between the times $t' \leq t$. The correlator determines stress fluctuations via approximations of mode coupling type. Effective potentials enter in the mode coupling approximations as familiar from density functional theory. Averages, like shear and normal stresses, but also distorted structure factors are then obtained from integrating through the transients in (generalized) Green-Kubo formulae. The Green-Kubo

4th International Symposium on Slow Dynamics in Complex Systems
AIP Conf. Proc. 1518, 134-142 (2013); doi: 10.1063/1.4794560

relation takes the form given that a time-dependent shear flow of rate $\dot\gamma(t)$ is applied $\dot\gamma(t)$ [7]

$$\sigma(t) = \int_{-\infty}^{t} dt'\ \dot\gamma(t')\, G(t,t'). \tag{1}$$

Equation (1) is formally exact, but highly complex as it is nonlinear in the shear rate. This arises from the nonlinear functional dependence of the shear modulus $G(t,t')$ on $\dot\gamma(t)$. Here $G(t,t')$ is a transient correlator of fluctuating transverse stresses. The standard mode coupling approximations are used on it, including the breaking of higher order correlation functions into products of lower order ones by which the density correlator $\Phi_{\mathbf{q}}(t,t')$ enters.

$$G(t,t') = \frac{k_B T}{16\pi^3} \int \frac{d\mathbf{k} k_x^2 k_y(t,t')}{k k(t,t')} \frac{S_k' S_{k(t,t')}'}{S_k^2}\, \Phi^2_{\mathbf{k}(t,t')}(t,t'). \tag{2}$$

Here, $S_k' = \partial S_k/\partial k$, with S_k the equilibrium structure factor. The advected wave vector, $\mathbf{k}(t,t') = (k_x, k_y + \gamma(t,t')k_x, k_z)^T$ for shear flow, captures the affine deformation by the strain $\gamma(t,t') = \int_{t'}^{t} ds \dot\gamma(s)$ accumulated between the two times $t' \le t$. The density correlator obeys a causally retarded integral equation where a friction kernel arises from the competition of particle caging and flow advection of fluctuations. The latter kernel is also approximated using ideas from quiescent MCT; see ref. 5 for a detailed derivation of the equations in the case of steady shearing, and ref. 9 for the detailed generalization to arbitrary homogeneous flows. The MCT equations of motion are fully specified by the equilibrium structure factor S_q and a single initial time scale. It is often connected to the short time diffusion coefficient. Equations (2) thus predicts the nonlinear rheology from equilibrium structural correlations, and neglects e.g. hydrodynamic interactions. MCT presumes that they only shift the time scale. In colloidal dispersions, hydrodynamic interactions also contribute a high-frequency viscosity η_∞, which can be accounted for writing

$$G(t,t') \to G^{\mathrm{MCT}}(t,t') + \eta_\infty\, \delta(t-t'). \tag{3}$$

Structural correlations at the peak of the structure factor dominate the microscopic ITT-MCT equations. They are connected with the wave vector inverse to the average particle separation. The spatially resolved equations for $\Phi_{\mathbf{q}}(t,t')$ can be simplified to a single one for a local density correlator $\Phi(t,t')$, because the dynamics on all length scales is coupled strongly (factorization theorem of MCT). In the resulting 'schematic model', the modulus is expressed by the transient correlator as

$$G(t,t') = v_\sigma(t,t')\, \Phi^2(t,t'). \tag{4}$$

The transient stress-stress correlation function $G(t,t',[\dot\gamma])$ depends on the full flow history arising from the time-dependent shear rate $\dot\gamma(t)$. In general, it depends on the two times corresponding to the underlying fluctuations separately. The strain-dependent function v_σ is an elastic coefficient which captures the coupling of stress to density fluctuations. It was set to a constant in the original formulation of the model [**?**]. In the microscopic theory, $G(t,t')$ is given by an integration over wave vectors, including nontrivial weights that depend on time since density fluctuations are advected by shear. To account for the dephasing of wavevector contributions, which make G negative in the microscopic theory, we let hte prefactor $v_\sigma(t,t')$ depend on time through the accumulated strain $\gamma(t,t') = \int_{t'}^{t} \dot\gamma(s)\, ds$,

$$v_\sigma(t,t') = v_\sigma^* \cdot \left(1 - \left(\frac{\gamma(t,t')}{\gamma^*}\right)^2\right) \exp\left(-\left(\frac{\gamma(t,t')}{\gamma^{**}}\right)^2\right). \tag{5}$$

Because of symmetry, the direction of the strain does not matter, leading to an even function $v_\sigma = v_\sigma(\gamma(t,t')^2)$. Equation (5) was justified by a comparison with fully microscopic ITT-MCT calculations in two dimensions in Ref. [11]. The single-mode density correlator (normalized to $\Phi(t,t) = 1 - \Gamma(t-t')$) is obtained from an equation of motion simplified from the full MCT equations by neglecting wave vectore dependences

$$\partial_t \Phi(t,t') + \Gamma\left(\Phi(t,t') + \int_{t'}^{t} ds\, m(t,s,t') \partial_s \Phi(s,t')\right) = 0. \tag{6}$$

Γ is the initina decay rate which sets the time-scale depending on instantaneous (hydrodynamic) correlations. At the glass transition, the stress fluctuations measured by m become as slow as the density fluctuations, and thus the time-dependence of the memory function is comparable to the one of the correlator. MCT formulates a self-consistent approximation where the friction kernel is a functional of the density correlator. In Ref. [12] the memory function is modeled as

$$m(t,s,t') = \hat h(t,t')\, h(t,s)\, [\, \nu_1 \Phi(t,s) + \nu_2 \Phi^2(t,s)\,]. \tag{7}$$

The 'vertices' ν_1 and ν_2 mimick the structure factor in the microscopic theory and are assumed to increase smoothly with increasing the importance of particle interactions. There is a bifurcation where a viscoelastic fluid becomes a plastically deformed glass, generalizating the idealized glass transition found in quiescent MCT. The parameter ε measures the distance of the quiescent thermodynamic statepoint from the bifurcation and thus is a crucial parameter, termed separation parameter. Negative values of ε correspond to fluid states and positive values to glass states. In the schematic model the vertices are conventionally modeled as $\nu_2 = 2$ and $\nu_1 = 2(\sqrt{2}-1) + \varepsilon/(\sqrt{2}-1)$. Without flow, the schematic model simplifies to the well known F_{12}-model,

originally introduced by Götze.[3] Under flow, the accelerated loss of memory caused by the flow is expressed by the $h,\hat{h}$-functions in the memory kernel (eqn 7). For simplicity, [12] $\hat{h} = h$ is assumed, which incorporates identically strain accumulated between t and t' as well as that between t and s. Symmetry [7] again requires the h-functions to be symmetric in strain:

$$h(t,t') = \frac{\gamma_c^2}{\gamma_c^2 + \gamma(t,t')^2}, \tag{8}$$

where the constant γ_c sets a characteristic magnitude for the accumulated strain.

The presented equations depend upon three scale parameters. The ν_σ gives the stress magnitude, Γ sets a short-time scale, and γ_c sets the strain scale. The separation parameter ε is a crucial parameter which gives the distance to the glass transition and the time-dependent shear rate $\dot{\gamma}(t)$ describes the flow.

RESULTS

Pertinent results are reviewed which were obtaind in computer simulations, experiments, and MCT calculations using the described schematic model. Brownian dynamics simulations in two dimensions and experiments on model core-shell microgels will be reviewed, because detailed comparisons with theory were performed.

Stress-strain curves after switch-on

The most simple time dependence in the applied shear flow, is switching on a constant shear rate at time $t = 0$. Figure 1 shows stress-strain curves from 2d simulations of Brownian hard disks for given shear rates and for two densities. Both densities are very close (below and above, respectively) to the critical density, $\varphi_c = 0.796$, where MCT locates an idealized glass transition [13]. Hopping processes, however, melt the computer glass. The Peclet number, defined as $Pe_0 \equiv \dot{\gamma}\, d_s^2/D_0$, measures the strength of the shear driven motion relative to the dilute Brownian diffusion, and should be small compared to unity for the theory to apply. More details on the simulation can be found in Ref. [11], whose presentation we follow.

Fig. 1 shows the stress vs strain curves after switch-on from simulation compared to fits using the schematic model. The stress vs strain curves show a stress overshoot for all densities and shear rates outside the linear response regime. The linear response regime only exists in fluid states, where it can be observed as long as the dressed Peclet number $Pe = \dot{\gamma}\tau_\alpha$ is small compared to unity. For small strains, the stress increases linearly with strain and a common elastic constant G_∞ can be observed, $\sigma \sim G_\infty \gamma$. For bare Peclet numbers approaching unity, the merging of short and long time processes results in a shift of the linear portion in the stress-strain curve.

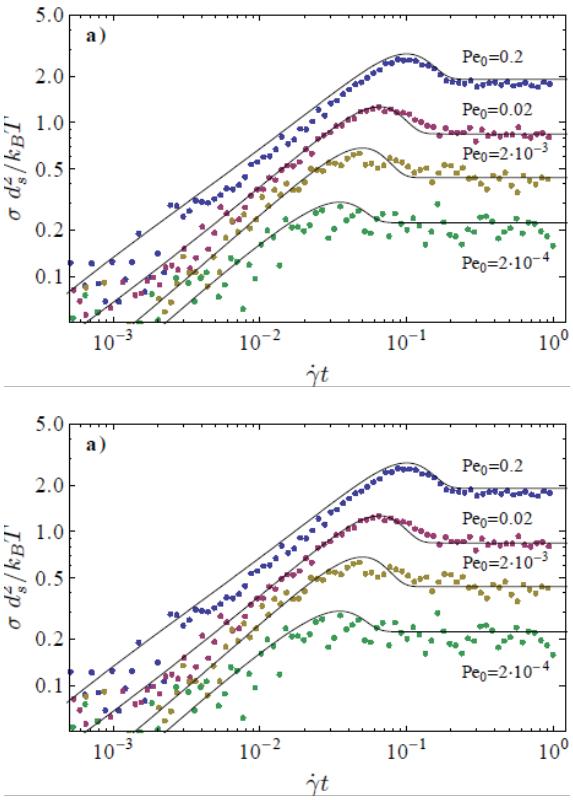

FIGURE 1. Stress vs strain curves from Brownian dynamics simulation in two dimensions; from Ref. [11]. *Disks* in *a)* are for $\varphi = 0.79$, and *squares* in *b)* for $\varphi = 0.81$; shear rates, converted to Peclet numbers, are as labeled. The *black* lines are fits using the $F_{12}^{(\dot{\gamma})}$ model.

The main outcome of this investigation is that the transient shear stress after switching on a fixed shear rate at time zero generically exhibits a maximum before settling on the stationary flow-curve value. It arises from negative stress correlations that build up when the intrinsic structural relaxation gets strongly affected by the shear driving. The transient dynamics initially follows the quiescent one, while it coincides with the stationary dynamics under flow at long times. Inbetween, it exhibits negative stress correlations for fluid and glass states as long as the shear rate exceeds the inverse α-relaxation time. Molecular dynamics simulations and confocal microscopy studies have indicated that the stress overshoot is accompanied by super-diffusive mean squared displacements [14]. Apparently, the negative stress correlations cause faster than diffusive particle motion, which takes place for averaged particle separations slightly

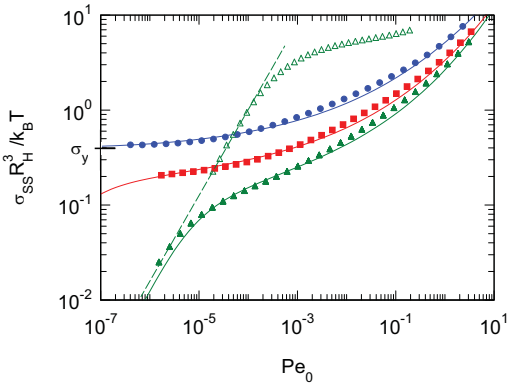

FIGURE 2. Experimentally measured flow curves[15] for three different temperatures, $T = 20.0°\mathrm{C}$ ($\phi_{\mathrm{eff}} = 0.57$, filled green upright triangles), $T = 18.0°\mathrm{C}$ ($\phi_{\mathrm{eff}} = 0.60$, filled red squares) and $T = 15.0°\mathrm{C}$ ($\phi_{\mathrm{eff}} = 0.65$, filled blue circles). Solid lines: theoretical fits to the data (see ref. 15). The open green upright triangles show $|G^*|$ at $\phi_{\mathrm{eff}} = 0.57$ from the applied Cox-Merz rule. The green dashed line is inserted as a guide line for the eye; from Ref. [10].

larger than the localization length in the quiescent glass, which itself compares well to Lindemann's length.

Stationary flow curves

As shown in the previous section, a stationary state is reached under applied shear rate for accumulated strains of the order of unity and even less. The resulting flow curve, viz. stress vs shear rate curve, is another simple and characteristic property of the nonlinear response of a colloidal system to flow.

In Fig. 2 we show typical flow curves measured in colloidal microgel dispersions from Ref. [15]. Data over a wider range of parameters are included in ref. [16], and more discussion can be found in ref. [17]; our presentation follows Ref. [10].

For small Peclet numbers the flow curve measured at $\phi_{\mathrm{eff}} = 0.57$ (at 20°C) shows a first Newtonian regime; the steady stress increases linearly in shear rate. As Pe_0 is increased we observe a decrease in viscosity, apparent as a sub-linear increase of the stress. At much higher shear rates a second Newtonian regime is approached. This flow curve is characteristic for a shear thinning fluid. The strong variation sets in already at shear rates far below their natural scale, $\mathrm{Pe}_0 \ll 1$. The cause is the structural relaxation, which leads to the dressed Peclet number $\mathrm{Pe} = \dot{\gamma}_0 \tau$ as a relevant parameter. The first Newtonian regime only holds for shear rates below $\mathrm{Pe} \leq 1$, where shear thinning sets in. The flow curve measured at the lower temperature 18°C ($\phi_{\mathrm{eff}} = 0.60$) displays a more pronounced region, where the stationary stress is constant. This holds except for the lowest shear rates, where the drop in the fitted curve, to the left of the experimental data, suggests the existence of a finite α-relaxation time which has shifted out of the experimental shear rate window. For the lowest temperature investigated, 15°C ($\phi_{\mathrm{eff}} = 0.65$), the flow curve exhibits a constant plateau down to the lowest values of Pe_0. The constant stress plateau corresponds to a finite dynamic yield stress, $\sigma_y = \sigma_{ss}(\dot{\gamma}_0 \to 0)$, which characterizes the yielding of a shear-melted glass. While the quiescent glass state is nonergodic and particles are localized, under arbitrarily slow flow, the system becomes ergodic and particles can diffuse in all directions including perpendicular to the flow direction.

Figure 2 contains fits from an ITT-MCT schematic model [15], which is a simplified version of the one used and discussed in the previous sections; it neglects the stress-overshoot phenomenon and simplifes $v_\sigma(t) \approx v_\sigma^*$. The model very well explains the data with a choice of fit parameters which qualitatively agree with the ones chosen for analyzing the Brownian dynamics simulations. Importantly, in Refs. [15, 10] it was shown that flow curves, large amplitude oscillatory shearing, and linear response moduli can be rationalized by the model using a single set of fit parameters.

It may be worth to mention that the widely used, phenomenological Cox-Merz rule has no basis for the nonlinear rheology close to a glass transition. It sets ad-hoc $|G^*(-i\omega)| = \sigma_{ss}(\dot{\gamma}_0 = \omega)$. The functional shapes of both functions, however, are different in a dense dispersion. Our data in Fig. 2 show this clearly. More importantly, the flow curve is characterized by the yield stress σ_y, while the elastic constant G_∞ characterizes the complex modulus G^*. Both are conceptually different quantities, which is not captured by the Cox-Merz rule.

Large amplitude oscillatory shearing

Another experimental protocol that displays key aspects of the nonlinear rheology of viscoelastic dispersions and yielding soft solids is an externally applied oscillatory shear strain of the form

$$\gamma(t) = \gamma_0 \sin(\omega t)\,, \tag{9}$$

introducing the parameters strain amplitude γ_0 and frequency ω. The response of the microgel system at long times is considered so that transient effects from switching on the strain have decayed; again, our presentation follows Ref. [10].

In Fig.3 we show the stress response measured in Brownian dynamics simulations of a binary hard-disc mixture in two dimensions. As the strain amplitude is

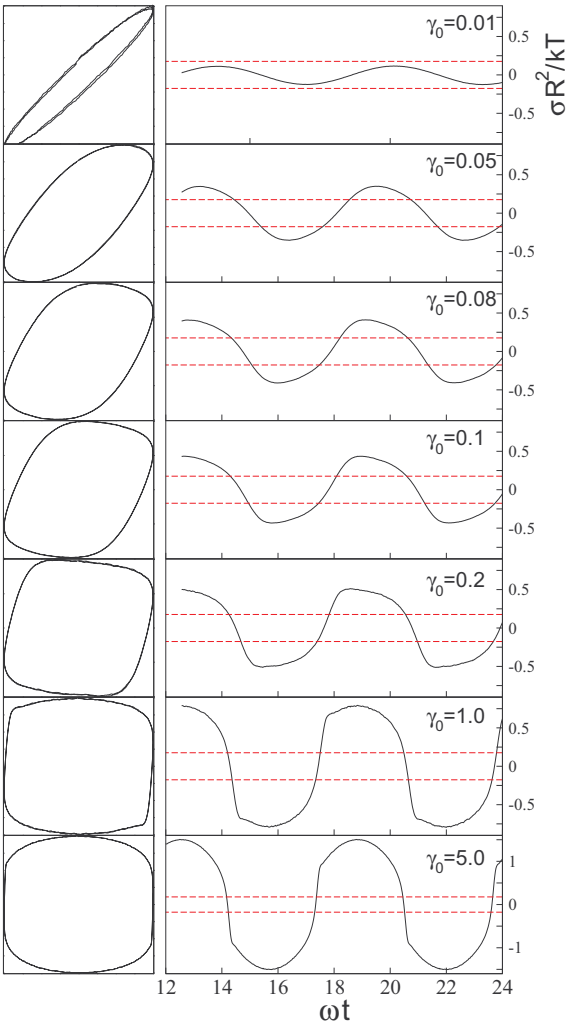

FIGURE 3. The stress response measured in Brownian dynamics simulations of a binary hard-disc mixture under oscillatory flow; from Ref. [15]. A size ratio 1 : 1.4 was used to supress crystallization. The considered strain amplitudes range from $\gamma_0 = 0.01$ to $\gamma_0 = 10$. The left column of figures shows the associated Lissajous curves illustrating the nonlinear character of the response. The simulations are performed at $\phi_{\rm tot} = 0.81$ (slightly beyond the glass transition, according to our simulation estimates). The Peclet number is $Pe_\omega = 0.05$).

increased the simulated stress evolves from a linear to a nonlinear response for $\gamma_0 > 0.03$. The time dependent signal becomes distorted away from a pure sinusoid when the peak of $\sigma(t)$ encounters the dynamic yield stress; it is included as red dashed lines in Fig.3. At this frequency Peclet number $Pe_\omega \equiv \omega\, d_s^2/D_0 = 0.05$, the nonlinear stress signal exhibits a flattened and asymmetric peak which is skewed to the left. Theory predicts that for even lower frequencies, the peak maximum should approach the yield stress value, but this could not be tested by simulation.

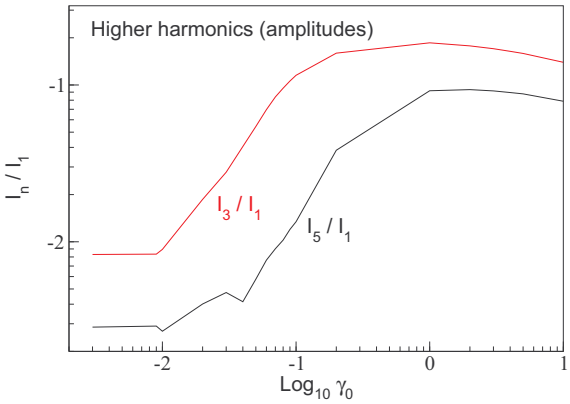

FIGURE 4. The normalized intensities of the third and fifth harmonic contributing to the nonlinear stress response shown in Figure.3; from Ref. [15].

In order to analyze more closely the stress signal, in Fig. 4 we show the intensities of the third and fifth harmonic as a function of γ_0. Higher order terms were found to be highly susceptable to the effects of statistical noise in the simulation data and have thus been omitted. Upon increasing the strain amplitude beyond $\gamma_0 = 0.03$ the system leaves the linear response regime and the contribution of the third harmonic grows. For strains exceeding around 0.1 the fifth harmonic also begins to play a significant role in determining the stress response. In keeping with schematic models predictions, both I_3/I_1 and I_5/I_1 exhibit a maximum, albeit more sharply peaked and shifted to slightly larger strain values approaching unity.

The full LAOS stress signal measured in microgel dispersions at a frequency in the β-window (0.01 Hz corresponding to the Peclet number $\mathrm{Pe}_\omega = 0.0025$) is given in the right panels of Fig. 5. The deformation varies from $\gamma_0 = 0.03$ in the linear regime to $\gamma_0 = 5$ deep in the nonlinear one. For small strain amplitudes, the linear viscoelastic behaviour is indicated by the nearly perfect sinusoidal stress $\sigma(t)$. It becomes distorted as γ_0 is increased. (Similar information can be obtained from the 'Lissajous curves' shown in the left panels of Fig. 5, which are parametric normalized strain-stress curves.[15]) For the low chosen frequency, the stress signal displays flattened asymmetric peaks at intermediate values of γ_0, consistent with a regime of cage breaking around $\gamma_0 = \gamma_c$. The schematic model calculations included in the figure are in good agreement with the experimental data. Data at higher frequencies show somewhat larger deviations from the model calculations.

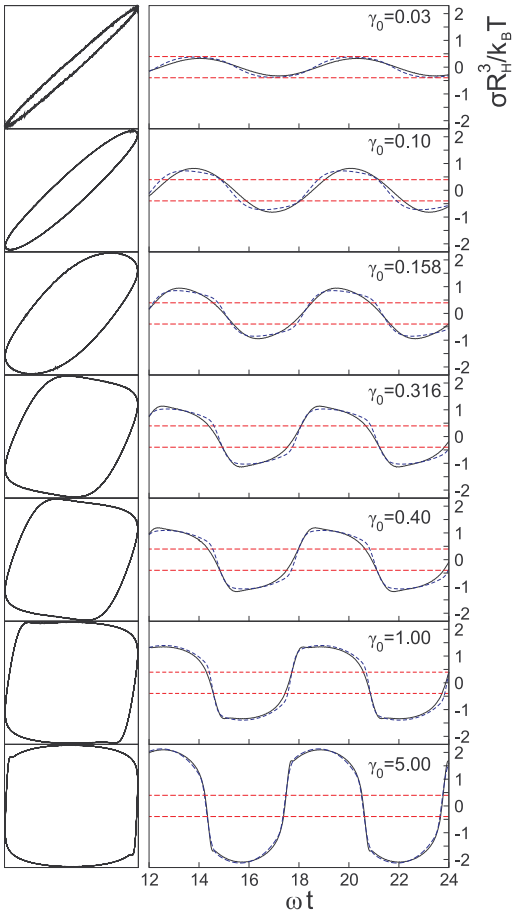

FIGURE 5. The stress response measured in LAOS experiments for strain amplitudes from $\gamma_0 = 0.03$ to $\gamma_0 = 5$ (black line) and the associated Lissajous figures illustrating the nonlinear character of the response. The experiments are performed at $T = 15.1°$C a glassy state and at a frequency of 1 Hz (corresponding to $\mathrm{Pe}_\omega = 0.02533$). At $\gamma_0 = 0.03$ the response is almost entirely elastic, emphasizing the proximity of the quiescent state to the glass transition. At $\gamma_0 = 5$ the system is almost purely viscous. The increase in dissipation with increasing γ_0 is reflected in the increasing area enclosed by the closed Lissajous curves. The yield stress is indicated by the broken red lines. Theoretical results are given by broken blue lines. Figure taken from Ref. [15].

Step strain

We now discuss numerical results found in the schematic model considering step strains; our presentation follows Ref. [18]. We start with the case of a single step strain. In the ideal glass phase ($\varepsilon > 0$), the quiescent-state correlation function does not decay but exhibits a finite long-time limit f_0. As a consequence, the memory kernel also does not decay. Moreover a

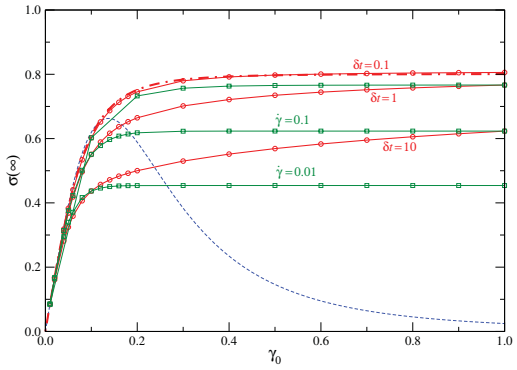

FIGURE 6. Stress $\bar{\sigma}(\infty)$ long after the application of a step strain with amplitude γ_0, obtained in the F_{12} model (with simplification $\nu_\sigma(t) = \nu_\sigma^*$) at the glass transition, $\varepsilon = 0$. Red and green curves differ in the modeling of the rapid flow variation during the time-resolved step. While all curves agree in the linear regime, green curves, which use a constant shear rate during the time-resolved step, exhibit a constant saturation stress more quickly than the red curves, which use a finite step-time; Figure taken from Ref. [18], where the curves are discussed in more detail.

step strain is unable to melt the glass on a permanent basis, so that a finite long-time limit exists also for the memory function and resulting correlator needed to compute the stress response to such a step. Accordingly, the stress response does not decay to zero but to a finite value $\bar{\sigma}(\infty)$. It is shown in Fig. 6 for a typical glass state as function of strain amplitude γ_0. A linear regime extends up to $\gamma_0 \approx \gamma_c$, indicating the response of an elastic solid, $\sigma = G_\infty \gamma_0$, where G_∞ is the glass plateau modulus. After that, a sublinear regime indicates plastic deformation. The precise result depends on the modeling of the step-strain, which taken literally as an infinitely rapid deformation would require an infinite shear rate $\dot{\gamma}$. This falls outside the range of validity of the theory, and also is not a reasonable description of a real step strain experiment on a colloidal dispersion. Resolving the rapidly varying shear flow during the 'step' strain deformation differently, gives quantitatively different results for the large amplitude step strain experiment. Qualitatively, however, in all cases the stress saturates at a constant value for large γ_0.

The large-γ_0 asymptote can be understood by recognizing that the response is unaffected by the imposed shear except for a narrow window at the time where the shear rate is just being switched. The schematic model describes strain-softening because of the plastic deformation incurred during the strain. There is no region of negative differential elasticity. However, it should be noted, that the schematic model used in the analysis in Ref. [18] excludes some of the anelastic deformation mechanisms present in the schematic model dis-

cussed in the theory section of this manuscript. The time-dependence of the stress vertex is neglected, $v_\sigma(t) = v_\sigma^*$, which will suppress the residual stress shown in Fig. 6 for large γ_0, possibly giving a non-monotonous curve with negative differential elasticity as found for a semi-microscopic MCT calculation in Ref. [6]

Double step strain

We now turn to the more interesting case of a double step strain, where the residual stress is due to a nonlinear combination of the two single steps; our presentation continues to follow Ref. [18].

There is a remarkable difference of the MCT model to the expectation from BKZ-type constitutive equations when the time Δt between the two steps is large enough. In the BKZ-type constitutive equations, the nonlinear superposition principle implies that the response to an arbitrary strain history can be constructed from those to single step-strain experiments. As a consequence, applying two large strains in opposite directions but such that the total strain $\gamma = 0$, gives no residual stress according to BKZ-type models, no matter how large the waiting time between the strains. In the MCT model, a physically more plausible prediction emerges. Whereas for $\Delta t \to 0$, the nonlinear superposition principle is formally recovered, for $\Delta t \gg \tau_0$, the residual stress $\bar\sigma(\infty)$ is not a function of $\gamma_0 + \gamma_1$ alone. Instead the result becomes independent of γ_0 if $|\gamma_1| \geq \gamma_c$. When the strain amplitude of the second step is large, the system approaches a steady-state flow during the second step, which erases all memory of the past deformation history, including everything related to the first ramp (no matter how large was γ_0). Thus, we obtain for $\gamma_1 \gg \gamma_c$ the result $\bar\sigma^{(2)}_{\gamma_0,\gamma_1}(\infty) \to \bar\sigma^{(1)}_{\gamma_1}(\infty)$. Only if the second step is small can there be any positive residual stress from the first step.

In the case of exactly canceling double step strains, $\gamma_1 = -\gamma_0$, Fig. 7 shows the residual stress normalized by the linear elastic stress, $\bar\sigma(\infty)/(G_\infty\gamma_0)$ as a function of γ_0. The results contrast strongly the class of constitutive equations based on the BKZ form, for which all the curves in Fig. 7 would be identically zero. In the linear response regime, $\gamma_0 \to 0$, the ratio $\bar\sigma(\infty)/\gamma_0$ does not vanish but attains a limiting value that depends on Δt. Around $\gamma_0 \approx \gamma_c$, a minimum occurs that becomes more pronounced if Δt is increased, until it saturates for time delays beyond the relaxation time of the single step-strain response. At large strains $\gamma_0 \geq \gamma_c$, $\bar\sigma(\infty)$ approaches the same saturating value as following a single step, which shows up here as a slowly decaying $1/\gamma_0$ asymptote at large strains that is independent of Δt.

The analysis of both single and double step strains within the schematic MCT approach to the rheology of colloidal glasses can be found in more detail in Ref. [18]. It considers generic yield-stress materials, whose response to flow includes a strong contribution from plasticity: structural rearrangements are caused by straining the material. Standard rheological constitutive equations of BKZ type can fail drastically in the description of such plastic materials. We have discussed this in terms of the residual stress $\sigma(\infty)$ remaining in a glass that has been subject to an exactly reversed double step strain. BKZ models predicts this residual stress to vanish. Within MCT, a finite residual stress remains: it is non-vanishing because plastic flow has taken place in the time between the strains,

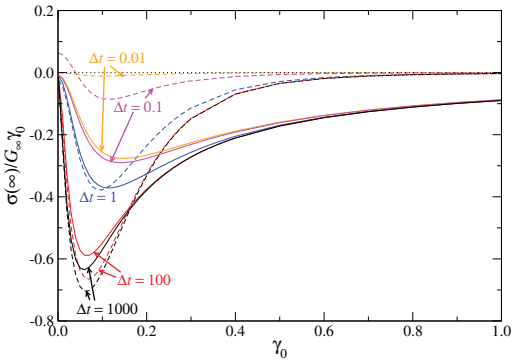

FIGURE 7. Stress recovery after exact step strain reversal: $\bar\sigma(\infty)$ as a function of and normalized by the elastic response $G_\infty\gamma_0$ for waiting times $\Delta t = 0.01$, 0.1, 1, 100, and 1000 (solid lines from top to bottom as labeled). The F_{12} model with $v_\sigma(t) = v_\sigma^*$ is used at $\varepsilon = 10^{-4}$; from Ref. [18], where a discussion of the other lines can be found.

Shear reversal

We now turn to the discussion of the Bauschinger effect, which also considers reversing deformations. The flow history is even simpler than in step strains, as in the studies following Bauschinger's pioneering work in the 19th century, the history dependence of the approach to the stationary state is tested. A simple example, the stress-strain curves for reversing shear rates was considered in Ref. [19], which we review in the following.

Figure 8 shows the main result of the computer simulation, viz. the stress–strain curves in the $|\sigma|$-versus-$|\gamma - \gamma_0|$ representation, i.e., shifted and inverted such that they all start from a stress-free state and display the behavior as a function of the additional strain imposed on this configuration. Curves for various γ_w are shown, where γ_w indicates the time when the flow was reversed. Reversing the flow in the stationary state is denoted by γ_w^s. Reversing the flow early after start-up, is denoted by

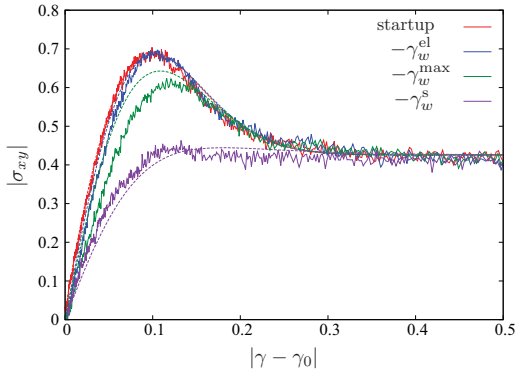

FIGURE 8. Linear plot of the stress-strain relation $|\sigma(|\gamma-\gamma_0|)|$ at fixed temperature and shear rate for various flow histories: starting from equilibrium (EQ, red line), after flow reversal in the steady state (S, purple), from the elastic regime (el, blue), and from the point of the stress overshoot (max, green); from Ref. [19].

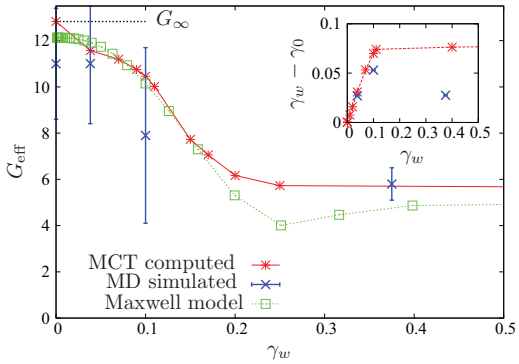

FIGURE 9. Linear stress responses $G_{\rm eff} = d\sigma/d\gamma|_{|\gamma-\gamma_0|=0.025}$ from simulation, fits of the schematic model, and a Maxwell model as labeled for various waiting strains γ_w; from Ref. [19]. The inset gives the strain $\gamma_w-\gamma_0$ required for the stress to reduce to zero after shear reversal.

$\gamma_w^{\rm el}$, and gives (almost) the identical stress vs strain curve as the original start-up curve. All stress-strain curves agree at large strains, confirming that the steady-state stress does not depend on the shear history. Comparing first the startup curve, $\gamma_w = 0$, with the one for reversal in the steady-state, $\gamma_w = \gamma_w^{\rm s}$, the Bauschinger effect becomes most apparent. The two curves differ in two main aspects: the initial linear slope at small deformations is lower, and the overshoot is gone in the curve corresponding to oppositely straining the pre-sheared configuration. Both these differences arise because the system undergoes plastic deformations during pre-shear: confining the pre-shear to small strains, $\gamma_w = \gamma_w^{\rm el}$, so that flow reversal takes place inside the initial elastic-deformation regime, the overshoot is maintained almost unchanged, as is the effective elastic coefficient extracted from the initial rise of the stress–strain curve. The cross-over between elasticity-dominated and plasticity-dominated pre-strain occurs gradually, as the curve for $\gamma_w = \gamma_w^{\rm max}$ exemplifies.

The solid lines in Fig. 8 represent the schematic-MCT model calculations. The line corresponding to $\gamma_w = 0$ is fitted in a standard procedure. All the other theory curves then follow from the structure of the ITT-MCT equations. They describe the computer-simulation data extremely well, and capture both the decrease of the overshoot and the decrease of the effective elastic coefficient.

The effective shear moduli, obtained as $G_{\rm eff} = d\sigma/d\gamma|_{|\gamma-\gamma_0|=0.025}$. display a characteristic crossover from elastic to plastic behavior. The results from the schematic MCT model (red and blue stars) are shown in Figure 9 together with the values extracted from the simulation data (blue crosses). The agreement is quite satisfactory, noting that only the initial value at $\gamma_w = 0$ is a result of a fitting procedure. One observes a marked decrease of $G_{\rm eff}$ around $\gamma_w \approx 0.1$, the position of the overshoot in the startup curve. Hence, pre-shear indeed softens the material, but only by plastic deformation.

CONCLUSIONS AND OUTLOOK

The results reviewed in this conference proceedings' contribution indicate that memory effects with very long memory times exist at the glass transition and can be manipulated by various external flow rates. Surprising effects, like the change of the effective elastic constants after flow reversal arise from the memory stored in the material. A dominating mechanism is shear thinning, that an applied shear rate enforces decay of correlations even in a state that would be a glass without flow. Stationary flow curves, which are equivalent to viscosity vs shear rate curves, directly show shear thinning. But also the stress traces in large amplitude oscillatory shearing are strongly affected by the effect of shear thinning. The importance of the dynamic yield stress and of the effective shear rate made up from the strain amplitude and the shear rate indicate this. Moreover, the elastic behavior of glass can be manipulated by shear, as shown for the case of step strains and shear flow reversal.

Mode coupling theory generalized to flowing states in the integrations through transients approach, captures the temporal memory effects in equations for the averaged responses. The nature of the spatial correlations needs not be specified in more detail, as density fluctuations on all wave vector scales participate in the slow structural relaxation. Therefore, a typical density correlator can be studied in simplified schematic models. The structure of the generalized Green-Kubo relations and of its equations of motion, where the complete flow history en-

ters in a highly nonlinear functional way, suffice to explain the generic phenomena at the glass transition under flow. The average affine motion of the particles with the flow introduces the external driving into the equations of motion of the density correlation functions. Asymptotic expansions show that the transient correlators in glass then become flow driven, as the internal structural relaxation has become irrelevant in comparison. Generalized Green-Kubo relations made quantitative with mode coupling approximations then enable one to calculate the stresses from the density correlators, which encode plastic deformations, and from effective fluctuation induced potentials. Simplified schematic models capture the universal phenomena which are independent of describing the spatial structure as long as all modes are strongly coupled at the glass transition.

ACKNOWLEDGMENTS

I cordially thank my colleagues for the very fruitful cooperations reviewed here, and acknowledge funding by the Deutsche Forschungsgemeinschaft through Research Unit FOR 1394, project P3, and Transregio SFB TR6, project A6.

REFERENCES

1. I. Gazuz, A. M. Puertas, Th. Voigtmann, and M. Fuchs, *Phys. Rev. Lett.* **102**, 248302 (2009).
2. D. Winter, J. Horbach, P. Virnau, and K. Binder, *Phys. Rev. Lett.* **108**, 028303 (2012).
3. W. Götze, *Liquids, Freezing and Glass Transition*, Amsterdam: North-Holland, 1991, p. 287.
4. M. Fuchs, and M. E. Cates, *Phys. Rev. Lett.* **89**, 248304 (2002).
5. M. Fuchs, and M. E. Cates, *J. Rheol.* **53**, 957–1000 (2009).
6. J. M. Brader, T. Voigtmann, M. E. Cates, and M. Fuchs, *Phys. Rev. Lett.* **98**, 058301 (2007).
7. J. M. Brader, M. E. Cates, and M. Fuchs, *Phys. Rev. Lett.* **101**, 138301 (2008), see also the associated Viewpoint article online in Physics **1**, 22 (2008).
8. J. M. Brader, *J. Phys.: Condens. Matter* **22**, 363101 (2010).
9. J. Brader, M. Cates, and M. Fuchs, *Phys. Rev. E* **86**, 021403 (2012).
10. M. Siebenbürger, M. Fuchs, and M. Ballauff, *Soft Matter* **8**, 4014–4024 (2012).
11. C. P. Amann, M. Siebenbürger, M. Krüger, F. Weysser, M. Ballauff, and M. Fuchs, *J. Rheol., in print* (2012).
12. J. M. Brader, T. Voigtmann, M. Fuchs, R. G. Larson, and M. E. Cates, *Proc. Natl. Acad. Sci. U.S.A.* **106**, 15186 – 15191 (2009).
13. F. Weysser, and D. Hajnal, *Phys. Rev. E* **83**, 041503 (2011).
14. J. Zausch, J. Horbach, M. Laurati, S. Egelhaaf, J. M. Brader, T. Voigtmann, and M. Fuchs, *J. Phys.: Condens. Matter* **20**, 404210 (2008).
15. J. Brader, M. Siebenbürger, M. Ballauff, K. Reinheimer, M. Wilhelm, S. Frey, F. Weysser, and M. Fuchs, *Phys. Rev. E* **82**, 061401 (2010).
16. M. Siebenbürger, M. Fuchs, H. H. Winter, and M. Ballauff, *J. Rheol.* **53**, 707–726 (2009).
17. J. J. Crassous, M. Siebenbürger, M. Ballauf, M. Drechsler, D. Hajnal, O. Henrich, and M. Fuchs, *J. Chem. Phys.* **128**, 204902 (2008).
18. Th. Voigtmann, J. M. Brader, M. Fuchs, and M. E. Cates, *Soft Matter* **8**, 4244 (2012).
19. F. Frahsa, A. K. Bhattacharjee, M. Fuchs, and T. Voigtmann, *J. Chem. Phys.* p. submitted (2012).